

Strain-Engineered Electronic Structure and Superconductivity in $\text{La}_3\text{Ni}_2\text{O}_7$ Thin Films

Yu-Han Cao^{1,*}, Kai-Yue Jiang^{2,*}, Hong-Yan Lu^{2,†}, Da Wang^{1,3,‡} and Qiang-Hua Wang^{1,3,§}

¹National Laboratory of Solid State Microstructures & School of Physics, Nanjing University, Nanjing 210093, China

²School of Physics and Physical Engineering, Qufu Normal University, Qufu 273165, China

³Collaborative Innovation Center of Advanced Microstructures, Nanjing University, Nanjing 210093, China

Recently, the films of the Ruddlesden-Popper (RP) nickelate superconductors, in which the $(\text{La},\text{Pr})_3\text{Ni}_2\text{O}_7$ system exhibits a remarkable transition temperature T_c exceeding 40 K, were synthesized at ambient pressure. We systematically investigate the band structures and electronic correlation effect to identify the key factors controlling superconductivity and pathways to enhance T_c . Based on density functional theory (DFT) calculations, we construct a bilayer two-orbital ($3d_{3z^2-r^2}$ and $3d_{x^2-y^2}$) tight-binding model for a series of in-plane compression mimicking the substrate effect. We find the band energy at the M point drops with the compression, leading to increase of the density of states at the Fermi level, in stark contrast to the behavior of the bulk under pressure. We then apply functional renormalization group (FRG) method to study the electronic correlation effect on the superconductivity. We find the s_{\pm} -wave pairing symmetry remains robust in the films, the same as the bulk. But somewhat surprisingly, for the films, we find T_c can be enhanced by reducing the in-plane lattice constant, increasing the out-of-plane lattice constant, or further electron-doping. These findings are consistent with the itinerant picture of the superconductivity induced by spin-fluctuations and provide theoretical support for further boosting T_c in future experiments.

Introduction. The discovery of the Ruddlesden-Popper (RP) structural bulk $\text{La}_3\text{Ni}_2\text{O}_7$ with T_c reaching the liquid nitrogen temperature regime [1] under high pressure, has attracted great interest recently. A large number of experimental [2–42] and theoretical [42–102] studies have been conducted to investigate the superconductivity, density wave and normal state electronic properties. However, the high-pressure condition has hindered further investigations or potential applications. Recently, two independent research teams achieved a significant breakthrough by successfully synthesizing RP bilayer thin films of $\text{La}_3\text{Ni}_2\text{O}_7$ (LNO) [103] and $\text{La}_{2.85}\text{Pr}_{0.15}\text{Ni}_2\text{O}_7$ (LPNO) [104], respectively, on SrLaAlO_4 (SLAO) substrate, both with T_c exceeding the McMillan limit at ambient pressure. This discovery has sparked a second tide in the community to investigate the RP nickelate films at ambient pressure.

By comparing these two experiments of LPNO and LNO films, we obtain the following information. (1) The in-plane lattice constant $a = 3.75 \text{ \AA}$ of the LPNO film is slightly smaller than the LNO film with $a = 3.77 \text{ \AA}$, which was suspected to be responsible for the higher T_c of LPNO film. But this tendency seems to be in contrast to the bulk LNO, for which higher pressure (hence smaller a) is found to reduce T_c [27]. On the other hand, the out-of-plane lattice constant c of the LPNO film is longer than the LNO film. However, at first glance, weaker out-of-plane hybridization (stemmed from longer c) seems to hamper superconductivity in many theories based on bilayer coupling. How to reconcile this paradox is actually one target of the present work. (2) Both films exhibit tetragonal space group, consistent with the appearance of superconductivity in bulk LNO under pressure, indicating the tetragonal lattice structure is indeed crucial for superconductivity in both bulk and films [105].

Further information can be obtained from later experiments. (3) The superconductivity was found to occur within the interfacial region about 1 unit cell (UC) from the SLAO substrate [106], indicating the effect of Sr (hole) doping in these two films. This hole-doping effect can explain the fact that the angle-resolved photoemission spectroscopy (ARPES) measurement [107] does not observe the small Γ -centered electron-like Fermi pocket as suggested by density functional theory calculations. This may suggest that hole-doping promotes the superconductivity. But later, the synthesis of $\text{La}_2\text{PrNi}_2\text{O}_7$ (*not* LPNO) film achieves higher T_c by removing the Sr-doping effect [108], partly consistent with the disappearance of the M -centered hole-like Fermi pocket [109]. This otherwise may suggest that electron-doping promotes superconductivity. Regarding to these progresses, the doping effect on electronic structure and superconductivity desires more systematic studies. (4) The ARPES study has revealed a nodeless superconducting gap on the Fermi pockets near the $\Gamma - M$ direction as dominated by the $d_{x^2-y^2}$ orbital [110], suggesting s - or s_{\pm} -wave pairing. Although this pairing symmetry is consistent with the bulk as predicted by many theoretical studies, the underlying superconducting mechanism of these theories differs significantly. The pressure or substrate dependence of both bulk and film materials hence provides a unique way to distinguish the superconducting mechanisms.

In this work, we systematically investigate the band structures and electronic correlation induced superconductivity of the LPNO and LNO films, aiming to uncover the key factors controlling T_c . Based on DFT calculations, we construct a bilayer two-orbital ($3d_{3z^2-r^2}$ and $3d_{x^2-y^2}$) tight-binding model. The tight-binding parameters and band structures are compared with the bulk to uncover their differences. We then apply functional

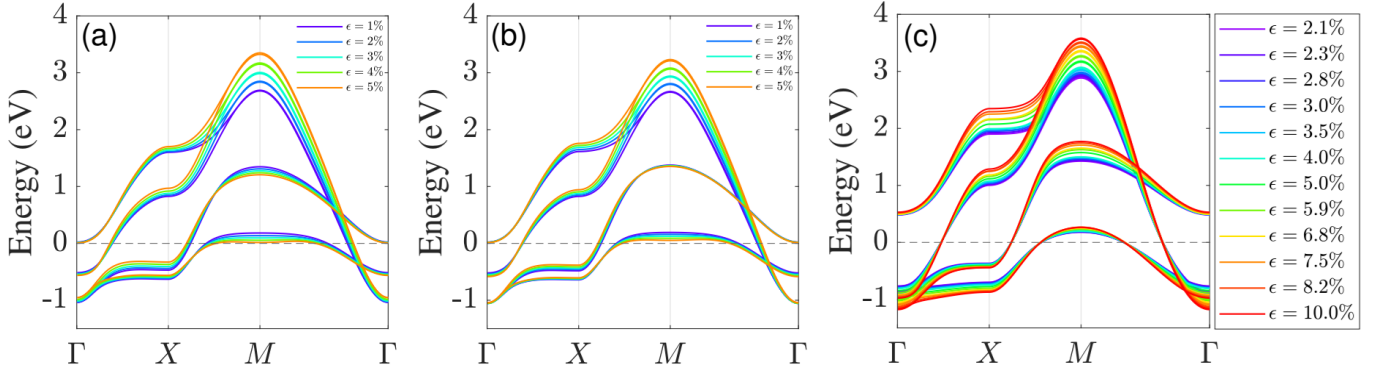


Figure 1. (a) Tight-binding band structures with $n = 1.25$ (electron number per Ni atom) under different in-plane compression ratio ϵ corresponding to the LPNO films, by fixing the out-of-plane expansion ratio $\epsilon_c = 0.5\epsilon$. (b) is similar to (a) but for the LNO films by fixing $\epsilon_c = 0$. (c) is similar to (a) but for the LNO bulk with $n = 1.5$ (converted from Ref. [111]).

renormalization group (FRG) to study the electronic correlation effect on the superconductivity. We find the s_{\pm} -wave pairing symmetry remains robust in the films, the same as its bulk counterpart. But somewhat surprisingly, for the films, we find T_c can be enhanced by (1) reducing the in-plane lattice constant, (2) increasing the out-of-plane lattice constant, or (3) further electron-doping, which can be understood by the itinerant picture of the superconductivity. These findings provide theoretical support for further enhancing T_c in future experiments.

Electronic structure & tight-binding model. The electronic structures of the LPNO and LNO films are calculated by DFT as implemented in the Vienna ab initio simulation package (VASP) on a half-UC thick $\text{La}_3\text{Ni}_2\text{O}_7$ film with the $I4/mmm$ space group. Due to the small concentration of Pr in LPNO, the two films are solely distinguished by different out-of-plane lattice constants while discarding the Pr doping. In experimental studies, LPNO and LNO thin films exhibit the approximately 2% of in-plane compression ratio compared to LNO bulk under ambient pressure, while the out-of-plane lattice constants show 1% elongation and remain virtually unchanged, respectively [103, 104]. Therefore, we set the in-plane compression ratio ϵ at 1% increments from 1% to 5% for both films. Correspondingly, the out-of-plane expansion ratio ϵ_c are set at 0.5% increments from 0.5% to 2.5% for LPNO, and fixed at 0% for LNO, respectively. With the method of maximally localized Wannier functions, we extract a bilayer two-orbital tight-binding model

$$H_0 = \sum_{i\delta, ab, \sigma} t_{\delta}^{ab} c_{ia\sigma}^{\dagger} c_{i+\delta b\sigma} + \sum_{ia\sigma} \varepsilon_a c_{ia\sigma}^{\dagger} c_{ia\sigma}, \quad (1)$$

where t_{δ}^{ab} is the hopping matrix element between the a orbital on site i and the b orbital on site $i + \delta$, σ represents spin, and ε_a is the on-site energy of the a -orbital. For simplicity, we use x and z to denote $3d_{x^2-y^2}$ and $3d_{3z^2-r^2}$ orbitals, respectively. The full DFT bands and

comparisons with the Wannier bands are shown in Supplemental Material (SM) [112]. All the tight-binding parameters are listed in Table S1 and S2 [112] for the two films, respectively.

The tight-binding band structures of LPNO and LNO films under different compression ratio ϵ are presented in Fig. 1(a) and Fig. 1(b), respectively. The Fermi energy corresponds to 1.25 electrons per Ni atom (labeled by n). As a comparison, the band structures of the bulk LNO with $n = 1.5$ for different ϵ (converted from hydrostatic pressure) [111] are shown in Fig. 1(c). Although the total band width increases for both films and bulk with increasing ϵ , the low energy (near the Fermi energy) bands exhibit quite different features. First, for both films, the energy band above the Fermi level at Γ drops very close to the Fermi energy, leading to a small electron-like Fermi pocket upon electron-doping, as shown in Fig. 2(a). Second, the hole band around M of both films becomes more flat than the bulk. Third, maybe the most intriguing feature of the films is the drop of the M -band with increasing ϵ , which is opposite to the tendency in the bulk. All these features lead to increase of the density of states (DOS) at the Fermi level in the films, reflecting the dis-

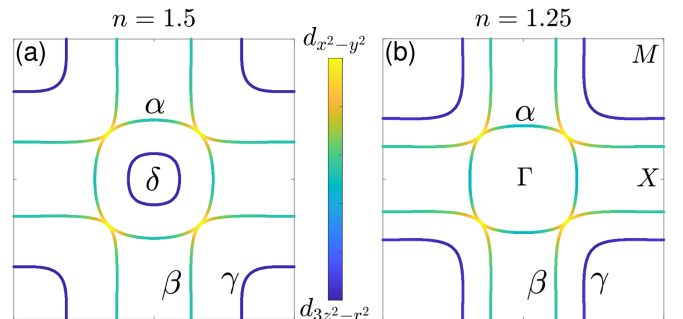


Figure 2. Fermi surfaces for the LPNO film under $\epsilon = 2\%$ for $n = 1.5$ in (a) and $n = 1.25$ in (b). The colors represent the orbital weights. The results for the LNO film are similar and not shown.

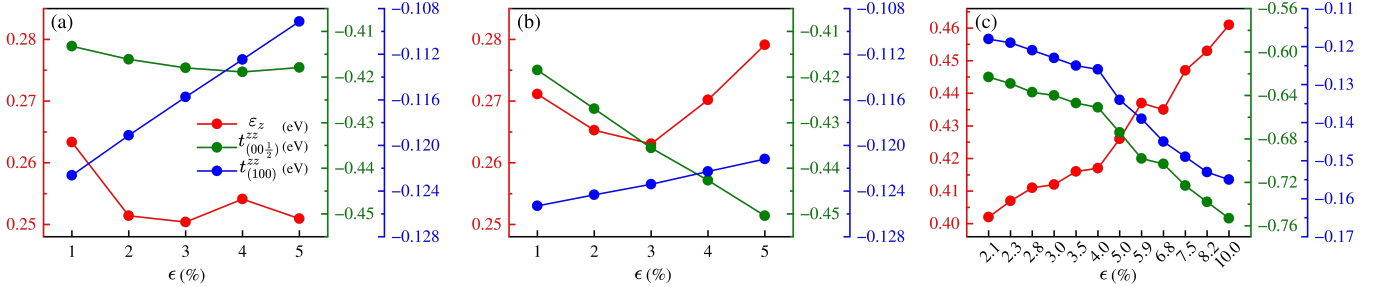


Figure 3. The onsite energy ε_z and hopping integrals $t_{(00\frac{1}{2})}^{zz}$ and $t_{(100)}^{zz}$ are plotted with respect to ϵ for the LPNO film (a), LNO film (b) and bulk LNO (c), respectively.

tinct effect of the in-plane strain versus the hydrostatic pressure on the band structure.

Since the in-plane lattice constant a is reduced for both films and bulk under pressure, the in-plane hopping amplitude between $d_{x^2-y^2}$ -orbital is enhanced for all these cases (see Table S1 and S2 in SM [112]). But because the out-of-plane lattice constant c increases for LPNO film, keeps invariant for LNO film, and drops for the bulk, the hopping integrals between $d_{3z^2-r^2}$ -orbital differ significantly among these three cases. In Fig. 3, we plot $t_{(00\frac{1}{2})}^{zz}$, $t_{(100)}^{zz}$ and ε_z versus the in-plane compression ratio ϵ for the two films and the bulk, respectively. For the bulk, both $t_{(00\frac{1}{2})}^{zz}$ and $t_{(100)}^{zz}$ are enhanced with increasing ϵ , hence, reducing c , as anticipated. But for both films, with increasing ϵ (reducing a), $t_{(100)}^{zz}$ is weakened unexpectedly. Moreover, for the LNO film, $t_{(00\frac{1}{2})}^{zz}$ is enhanced although c keeps invariant, while for the LPNO film, $t_{(00\frac{1}{2})}^{zz}$ is slightly enhanced although c increases. These counter-intuitive results come from the narrowing of the effective Wannier orbital carrying the $d_{3z^2-r^2}$ symmetry with increasing ϵ , uncovering a fundamental difference between the films upon in-plane strain and the bulk under hydrostatic pressure. With these results, we can understand the drop of M -band with increasing ϵ . At M , the lowest band comes from the bonding state of the z -orbitals, with the energy given by $\varepsilon_z + t_{(00\frac{1}{2})}^{zz} - 4t_{(100)}^{zz}$ up to the nearest neighbor hopping. For the bulk under pressure, the M -band grows up mainly due to the increase of ε_z , while for the films, the M -band drops mainly due to the hopping changes. The anomalous variation of t_{δ}^{zz} under in-plane strain is a peculiar property of the films [113–116].

Electronic correlation & superconductivity. Next, we investigate electronic correlation induced superconductivity by considering the atomic multi-orbital Coulomb interactions

$$H_I = \sum_{i,a < b, \sigma\sigma'} \left(U' n_{ia\sigma} n_{ib\sigma'} + J_H c_{ia\sigma}^\dagger c_{ib\sigma} c_{ib\sigma'}^\dagger c_{ia\sigma'} \right) + \sum_{ia} U n_{ia\uparrow} n_{ia\downarrow} + \sum_{i,a \neq b} J_P c_{ia\uparrow}^\dagger c_{ia\downarrow} c_{ib\downarrow}^\dagger c_{ib\uparrow}, \quad (2)$$

where U is the intra-orbital Hubbard repulsion, U' is the inter-orbital Coulomb interaction, J_H is the Hund's coupling, and J_P is the pair hopping interaction. As usual, we adopt the Kanamori relations: $U = U' + 2J_H$ and $J_H = J_P$ [117]. The two independent interaction parameters are chosen as $U = 3$ eV and $J_H = 0.3$ eV throughout this work.

To investigate electronic correlation properties, we employ the singular-mode FRG (SM-FRG) method, which is an unbiased approach for analyzing system instabilities by studying the flow of the one-particle-irreducible four-point vertex Γ_Λ versus a running infrared cutoff energy scale Λ while neglecting the self-energy and frequency-dependence in our approach. The vertex Γ_Λ can be reexpressed as scattering matrices between fermion bilinears in superconductivity (SC), spin-density-wave (SDW), and charge-density-wave (CDW) channels. Through iterative solution of the FRG flow equation, we monitor the negative leading singular value S_Λ of the scattering matrices versus Λ . At $\Lambda_c \sim T_c$, the first divergence of the S_Λ among the three channels indicates an instability to form a long range order. More technical details can be found in Refs. [44, 111, 118–123].

In Fig. 8, we present typical SM-FRG flows of S^{-1} versus Λ for three values of $(\epsilon, n) = (2\%, 1.25)$, $(3\%, 1.25)$ and $(2\%, 1.5)$, respectively, for the LPNO film. The results for the LNO film are similar and can be found in Fig. S3 in the SM [112]. At high Λ , the interactions are not renormalized, and thus the flows for the three cases of (ϵ, n) merge together. Due to the bare repulsive Coulomb interactions, the SDW channel dominates while the attractive SC channel has not been established. As Λ reduces, the CDW channel is significantly weakened due to Coulomb screening while the SDW channel keeps almost the same. When Λ reduces below ~ 1 eV, off-site spin correlations are established and enhance the SDW channel, which further induce the CDW and SC channels due to inter-channel overlap in the spirit of spin-fluctuation induced superconductivity. After the attractive SC interaction is established, the SC channel grows up faster than the other two channels due to Cooper instability, also known as the Kohn-Luttinger mechanism

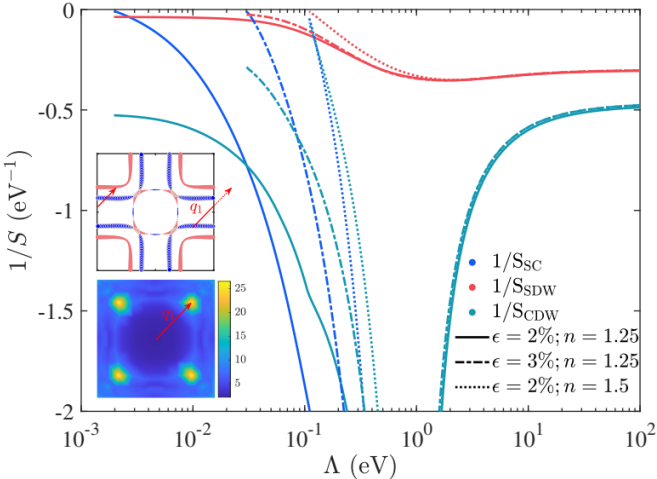


Figure 4. SM-FRG flows of S^{-1} versus Λ in the SC, SDW and CDW channels of LPNO film, respectively, at $(\epsilon, n) = (2\%, 1.25)$, $(3\%, 1.25)$ and $(2\%, 1.5)$. The upper subset plots the gap function on the Fermi surfaces with the pink (blue) color indicating the positive (negative) sign and the size indicating the magnitude of the gap function. The lower subset presents the leading negative $|S(\mathbf{q})|$ in the SDW channel. Both the subsets are obtained at $(\epsilon, n) = (2\%, 1.25)$.

[124]. For $(\epsilon, n) = (2\%, 1.25)$, the SC channel diverges (S^{-1} approaches zero) first, indicating that the system undergoes a phase transition into the superconductivity phase. By analyzing the eigenmode of the SC channel, we find that the real-space pairing is mainly dominated by local inter-layer pairing between $d_{3z^2-r^2}$ orbitals. More pairing components for different (ϵ, n) can be found in Fig. S4, Table S3 and Table S4 in the SM [112]. In the upper subset of Fig. 8, we plot the superconducting gap function projected onto the Fermi surface, from which the s_{\pm} -wave pairing symmetry is clearly seen. To analyze the pairing mechanism, we plot the momentum dependence $S(\mathbf{q})$ of the SDW channel in the lower inset of Fig. 8, which exhibits peaks at momentum $\mathbf{q}_1 = (5/8, 5/8)\pi$, up to C_{4v} symmetry. The momentum \mathbf{q}_1 can connect the Fermi surface with opposite sign gap functions, showing that the superconductivity is induced by spin fluctuations. For $(\epsilon, n) = (3\%, 1.25)$, the SM-FRG flows are qualitatively similar to the above, but with a higher critical energy scale Λ_c and stronger SDW channel. This indicates that larger ϵ enhances spin fluctuations, and thereby promotes T_c . For $(\epsilon, n) = (2\%, 1.5)$, although the SC fluctuation is stronger, the SDW channel diverges first and prevents the occurrence of superconductivity.

We have performed more calculations for a series of the in-plane strain ϵ and electron density n . The resulting T_c versus ϵ by fixing $n = 1.25$ for both films are plotted in Fig. 5(a). As a comparison, the FRG results for the bulk are also presented [111], which are consistent with the experiment [27]. Strikingly, we find that the T_c of both films are enhanced with increasing ϵ , in stark contrast to

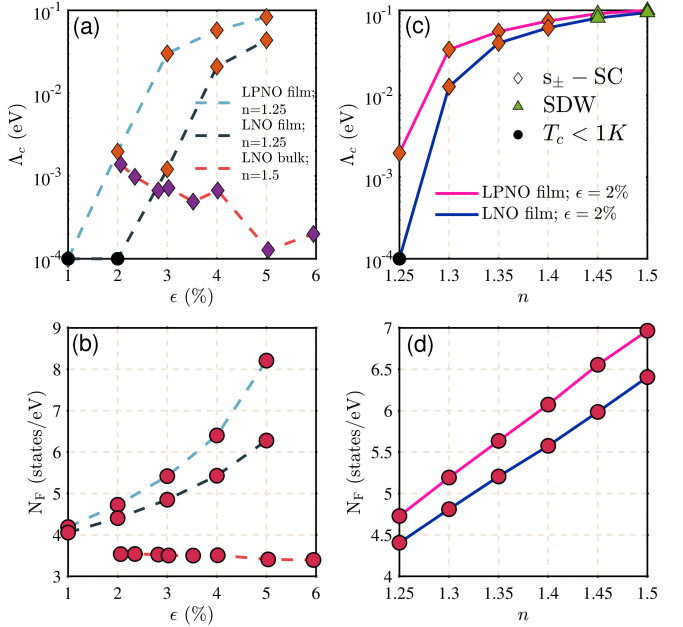


Figure 5. (a) Phase diagram of T_c ($T_c \sim \Lambda_c$) versus ϵ of the LPNO film, LNO film and LNO bulk, respectively. (b) DOS at the Fermi level (N_F) corresponding to (a). (c) Phase diagram of T_c versus n of the LPNO and LNO films under $\epsilon = 2\%$. (d) DOS N_F corresponding to (c).

the suppression of T_c in the bulk. Such an opposite trend shows a fundamental distinction between the two ways of band engineering via pressure. How to understand this difference? We attribute it mainly to the qualitatively different behavior of the DOS at the Fermi level N_F , as shown in Fig. 5(b). As discussed above, it stems directly from the distinct energy shift of the M -band with ϵ . Another striking feature is the theoretical T_c of the films can be higher than the bulk if higher in-plane strain can be realized experimentally on suitable substrate. Of course, the theoretical T_c should be understood as the pairing temperature. Phase fluctuation in the 2D films may further reduce it to the Kosterlitz–Thouless transition temperature.

It is also interesting to compare the two films directly. Note that the LPNO film has higher T_c than the LNO film for the same ϵ , due to higher DOS for the LPNO film although its out-of-plane lattice constant c is larger. This result is actually consistent with the experiments [103, 104]. We also examine the doping dependence of T_c , which is plotted versus n at fixed $\epsilon = 2\%$ in Fig. 5(c). Upon electron-doping with increasing n , the value of T_c grows up for both films. Again, this is consistent with the variation of the DOS N_F as shown in Fig. 5(d). Of course, as shown above, for large enough n , the system enters the SDW phase and hampers the formation of superconductivity. Here, both the strain and doping dependences of T_c can be understood by the itinerant picture of superconductivity. If confirmed by experiments, these features

can be used to identify the itinerant pairing mechanism in RP nickelate superconductors.

Conclusion. We systematically investigate the electronic band structures and correlation effects of the LPNO and LNO films. By DFT, we construct a bilayer two-orbital tight-binding model, uncovering the distinction of films relative to their bulk counterpart. Then by FRG, we investigate the electronic correlation induced superconductivity. We find the s_{\pm} -wave pairing symmetry remains robust in the films, the same as the bulk. For the films, we find T_c can be enhanced by reducing the in-plane lattice constant, increasing the out-of-plane lattice constant, or electron-doping. These findings support the itinerant picture of the superconductivity and offer theoretical support for further increasing T_c of the bilayer RP nickelates in future experiments.

Finally, it should be mentioned that our calculations are performed on the LPNO [104] and LNO [103] films,

and may not be workable for the $\text{La}_2\text{PrNi}_2\text{O}_7$ film [108], for which the M -pocket is not observed by ARPES [109]. If the M -pocket falls below the Fermi level, then we expect hole-doping can make it reappear to enhance T_c following the itinerant picture of superconductivity, since the contribution of the M -pocket to the DOS on the Fermi level is considerably large.

Acknowledgments. This work is supported by National Key R&D Program of China (Grants No. 2024YFA1408100, No. 2022YFA1403201), National Natural Science Foundation of China (Grants No. 12074213, No. 12374147, No. 12274205, No. 92365203), and Major Basic Program of Natural Science Foundation of Shandong Province (Grant No. ZR2021ZD01).

Data availability. The data that support the findings of this article are not publicly available. The data are available from the authors upon reasonable request.

Supplemental Materials

FIRST-PRINCIPLES CALCULATION RESULTS

First-principles calculation details

The calculations of structural relaxations and band structures for half-UC LNO thin film under different compressive strains are performed by density functional theory (DFT) calculations as implemented in Vienna *ab initio* simulation package (VASP) [125]. The projector augmented-wave (PAW) [126] method and the generalized gradient approximation (GGA) of Perdew-Burke-Ernzerhof (PBE) [127] exchange-correlation functional are adopted. The La $5s^25p^65d^16s^2$, Ni $3d^84s^2$, and O $2s^22p^4$ configurations are treated as valence electrons. The cutoff energy of plane-wave is set as 500 eV in all calculations. The total energies and force are well converged within 10^{-6} eV and 10^{-2} eV/Å, respectively. The Γ -centered $9 \times 9 \times 1$ k -point grid is used for both the structural relaxation and self-consistent calculations. Subsequently, to construct a bilayer two-orbital tight-binding model, the maximally localized Wannier functions (MLWF) [128, 129] of LNO thin film with $3d_{3z^2-r^2}$ and $3d_{x^2-y^2}$ orbitals on each Ni atom are extracted by the Wannier90 code [130], and the $18 \times 18 \times 1$ k -point grid is used for wannierization. The good overlapping between DFT and Wannier band structures indicates the high quality of Wannier functions, which is displayed in Fig. 6. In addition, the main tight-binding parameters extracted by Wannier90 are displayed Fig. 7, Table I and Table II.

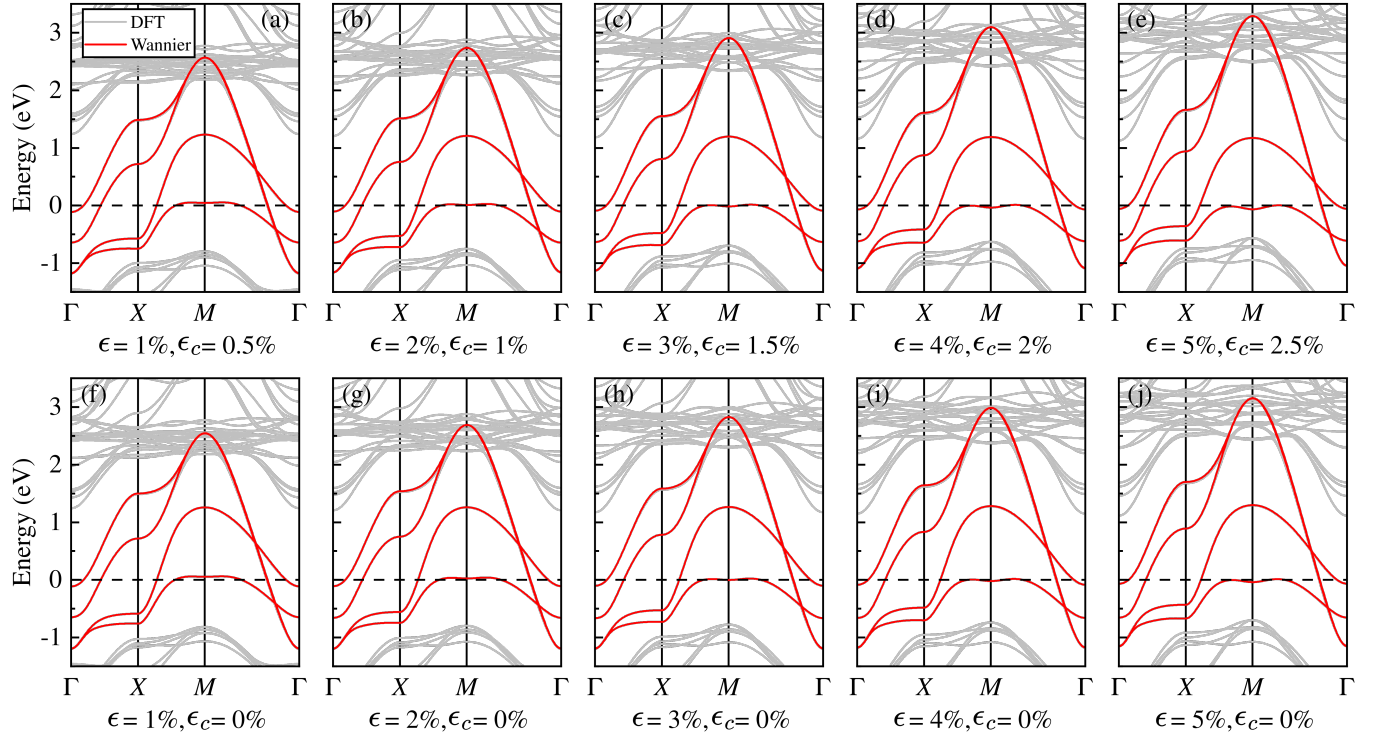


Figure 6. Comparison of DFT (grey line) and Wannier (red line) band structure corresponding to the LPNO (a-e) and LNO (f-j) films under different compressive strains.

Main tight-binding parameters under different compressive strains

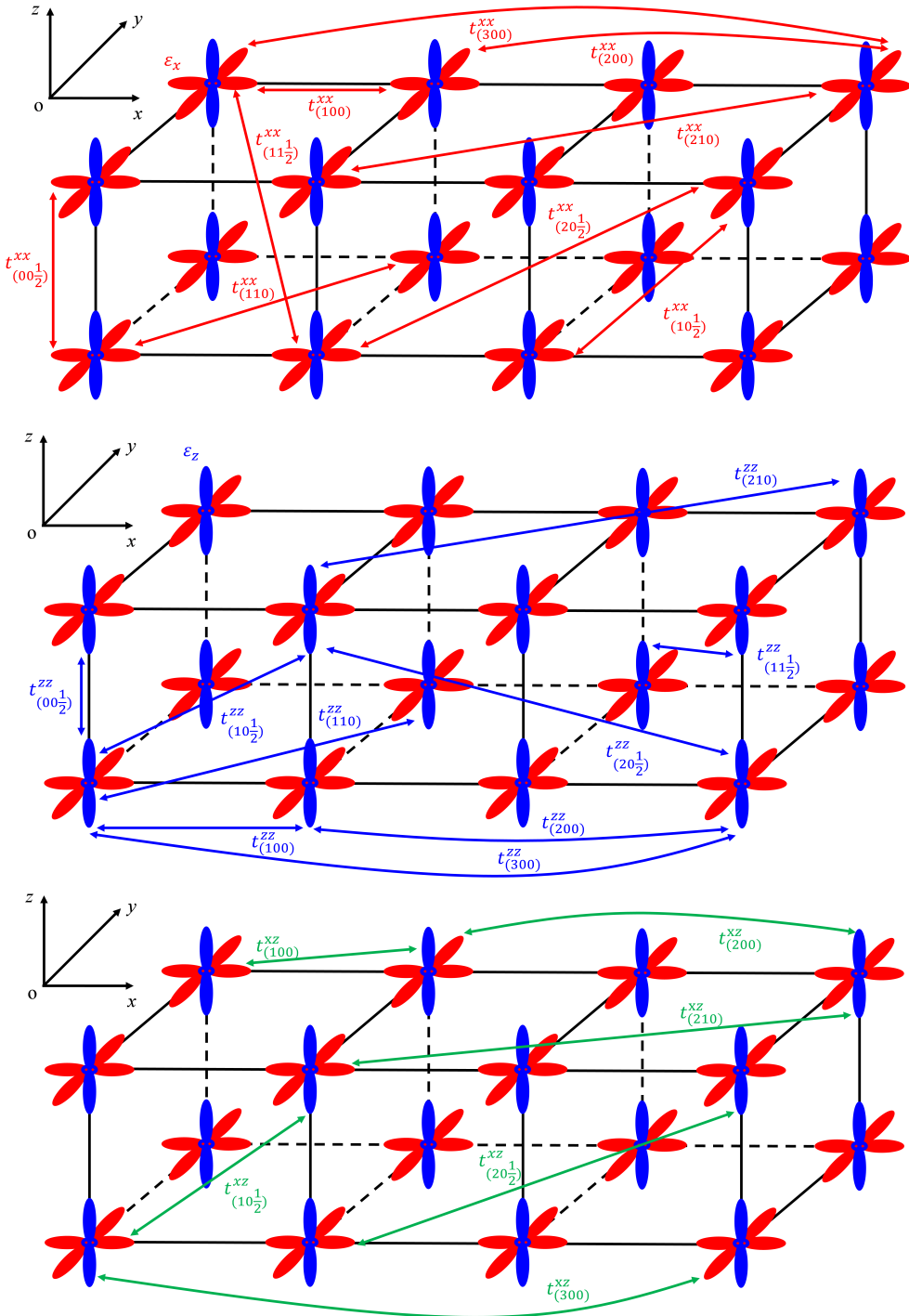


Figure 7. Schematic diagram for all parameters of the tight-binding model.

Table I. On-site energies ε_a and hopping integrals t_δ^{ab} of the bilayer two-orbital tight-binding model corresponding to LPNO thin film under different compressive strains. Here, x and z denote the $3d_{x^2-y^2}$ and $3d_{3z^2-r^2}$ orbital, respectively. Note that the vertical interlayer distance is assigned as $\frac{1}{2}$. The unit of ε_a and t_δ^{ab} is eV.

	$\epsilon=1\%, \epsilon_c=0.5\%$	$\epsilon=2\%, \epsilon_c=1\%$	$\epsilon=3\%, \epsilon_c=1.5\%$	$\epsilon=4\%, \epsilon_c=2\%$	$\epsilon=5\%, \epsilon_c=2.5\%$
ε_x	0.612463	0.712498	0.821973	0.948081	1.078286
ε_z	0.263342	0.251385	0.250385	0.254097	0.250916
$t_{(00\frac{1}{2})}^{zz}$	-0.413269	-0.416136	-0.417995	-0.418873	-0.417938
$t_{(00\frac{1}{2})}^{xx}$	0.000437	0.000001	0.000091	-0.000827	-0.000906
$t_{(100)}^{xx}$	-0.442817	-0.460940	-0.477479	-0.494620	-0.511621
$t_{(100)}^{zz}$	-0.122626	-0.119119	-0.115749	-0.112470	-0.109135
$t_{(100)}^{xz}$	0.212010	0.211878	0.211504	0.210866	0.209497
$t_{(10\frac{1}{2})}^{xx}$	-0.001026	-0.001219	-0.001526	-0.001485	-0.001685
$t_{(10\frac{1}{2})}^{xz}$	-0.033615	-0.034944	-0.036460	-0.037885	-0.039462
$t_{(10\frac{1}{2})}^{zz}$	0.039244	0.039238	0.039090	0.038898	0.038807
$t_{(110)}^{xx}$	0.074050	0.075795	0.076848	0.078037	0.078893
$t_{(110)}^{zz}$	-0.021513	-0.021161	-0.020978	-0.020753	-0.020356
$t_{(11\frac{1}{2})}^{xx}$	0.003667	0.003907	0.004215	0.004825	0.005300
$t_{(11\frac{1}{2})}^{zz}$	0.001746	0.001445	0.001455	0.001144	0.000698
$t_{(200)}^{xx}$	-0.051020	-0.053800	-0.056179	-0.059085	-0.062117
$t_{(200)}^{zz}$	-0.009686	-0.010302	-0.010852	-0.011420	-0.012308
$t_{(200)}^{xz}$	0.016726	0.017444	0.018209	0.019199	0.020451
$t_{(20\frac{1}{2})}^{xx}$	-0.003311	-0.003349	-0.003369	-0.003545	-0.003645
$t_{(20\frac{1}{2})}^{zz}$	-0.004803	-0.005019	-0.005475	-0.005933	-0.00641
$t_{(20\frac{1}{2})}^{xz}$	0.003491	0.003744	0.003964	0.004285	0.004779
$t_{(210)}^{xx}$	-0.004737	-0.004792	-0.004711	-0.004814	-0.004814
$t_{(210)}^{zz}$	-0.000759	-0.000680	-0.000695	-0.000538	-0.000421
$t_{(210)}^{xz}$	0.002223	0.002105	0.001893	0.001545	0.001233
$t_{(300)}^{xx}$	-0.012850	-0.013165	-0.013874	-0.014273	-0.014993
$t_{(300)}^{zz}$	-0.002167	-0.001944	-0.001592	-0.001414	-0.001117
$t_{(300)}^{xz}$	0.006197	0.006203	0.006142	0.006256	0.006273

Table II. On-site energies ε_a and hopping integrals t_δ^{ab} of the bilayer two-orbital tight-binding model corresponding to LNO thin film under different compressive strains. Here, x and z denote the $3d_{x^2-y^2}$ and $3d_{3z^2-r^2}$ orbital, respectively. Note that the vertical interlayer distance is assigned as $\frac{1}{2}$. The unit of ε_a and t_δ^{ab} is eV.

	$\epsilon=1\%, \epsilon_c=0\%$	$\epsilon=2\%, \epsilon_c=0\%$	$\epsilon=3\%, \epsilon_c=0\%$	$\epsilon=4\%, \epsilon_c=0\%$	$\epsilon=5\%, \epsilon_c=0\%$
ε_x	0.592366	0.671492	0.749354	0.847526	0.954883
ε_z	0.271121	0.265276	0.263073	0.270183	0.279125
$t_{(00\frac{1}{2})}^{zz}$	-0.418465	-0.426960	-0.435548	-0.442643	-0.450407
$t_{(00\frac{1}{2})}^{xx}$	0.000600	0.000114	-0.000295	-0.000490	-0.000229
$t_{(100)}^{xx}$	-0.442173	-0.459573	-0.475229	-0.492042	-0.508735
$t_{(100)}^{zz}$	-0.125291	-0.124333	-0.123394	-0.122272	-0.121186
$t_{(100)}^{xz}$	0.213847	0.215794	0.217339	0.2184890	0.219043
$t_{(10\frac{1}{2})}^{xx}$	-0.001056	-0.001101	-0.001211	-0.001364	-0.00157
$t_{(10\frac{1}{2})}^{xz}$	-0.033859	-0.035642	-0.037368	-0.039112	-0.040918
$t_{(10\frac{1}{2})}^{zz}$	0.040132	0.040913	0.041842	0.042877	0.0438080
$t_{(110)}^{xx}$	0.073732	0.074952	0.075868	0.076741	0.077328
$t_{(110)}^{zz}$	-0.021844	-0.021975	-0.022272	-0.022267	-0.022287
$t_{(11\frac{1}{2})}^{xx}$	0.003673	0.004131	0.004596	0.005083	0.005246
$t_{(11\frac{1}{2})}^{zz}$	0.001744	0.001753	0.001668	0.001246	0.000937
$t_{(200)}^{xx}$	-0.050764	-0.053063	-0.055063	-0.057675	-0.060372
$t_{(200)}^{zz}$	-0.009568	-0.010011	-0.010308	-0.010915	-0.011707
$t_{(200)}^{xz}$	0.016588	0.017084	0.0177390	0.018570	0.0195370
$t_{(20\frac{1}{2})}^{xx}$	-0.003429	-0.003549	-0.003788	-0.004057	-0.004105
$t_{(20\frac{1}{2})}^{zz}$	-0.004992	-0.005415	-0.005988	-0.006433	-0.006962
$t_{(20\frac{1}{2})}^{xz}$	0.003650	0.004085	0.004293	0.004671	0.005282
$t_{(210)}^{xx}$	-0.004722	-0.004643	-0.004759	-0.004680	-0.004688
$t_{(210)}^{zz}$	-0.000739	-0.000664	-0.000660	-0.000586	-0.000461
$t_{(210)}^{xz}$	0.002248	0.002053	0.001771	0.001522	0.001297
$t_{(300)}^{xx}$	-0.012858	-0.013182	-0.013816	-0.014257	-0.015030
$t_{(300)}^{zz}$	-0.002294	-0.002117	-0.001846	-0.001634	-0.001446
$t_{(300)}^{xz}$	0.006290	0.006248	0.006327	0.006385	0.006411

SINGULAR-MODE FUNCTIONAL RENORMALIZATION GROUP

SM-FRG flows of LNO film

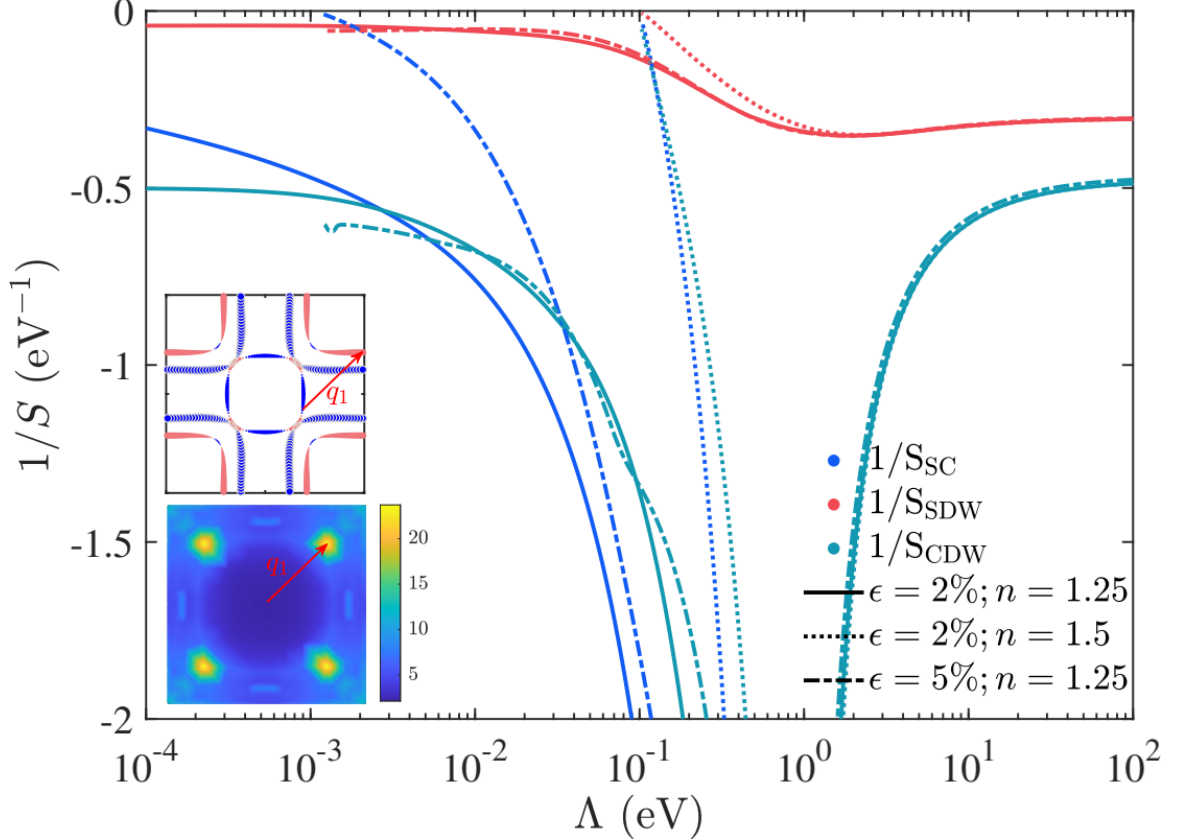


Figure 8. SM-FRG flows of S^{-1} versus Λ in the SC, SDW and CDW channels of LNO film, respectively, at $(\epsilon, n) = (2\%, 1.25)$, $(5\%, 1.25)$ and $(2\%, 1.5)$. The upper subset plots the gap function on the Fermi surfaces with the pink (blue) color indicating the positive (negative) sign and the size indicating the magnitude of the gap function. The lower subset presents the leading negative $|S(\mathbf{q})|$ in the SDW channel. Both the subsets are obtained at $(\epsilon, n) = (2\%, 1.25)$.

Real space superconducting pairing components

The SC pairing function can be obtained directly from the fermion bilinear singular mode of the diverging SC channel. The SC pairings operator in real space is written as $H_{SC} = \sum_{i\delta,ab} \Delta_\delta^{ab} c_{ia\uparrow}^\dagger c_{i+\delta b\downarrow}^\dagger + h.c.$, where a and b denotes the orbital, $\delta = 0, 1, 2$ denote the on-site, on vertical bond and on in-plane nearest-neighbor bond, respectively. The primary superconducting pairing components are shown in Fig. 9, where $u_{0,1,2}$ and $v_{0,1,2}$ denotes Δ_δ^{zz} and Δ_δ^{xx} , respectively. We also display the primary superconducting pairing components for $(U, J_H) = (3, 0.3)$ eV of LPNO and LNO films under different in-plane lattice constant compression ratios and $n = 1.25$ in Table III and Table IV, respectively.

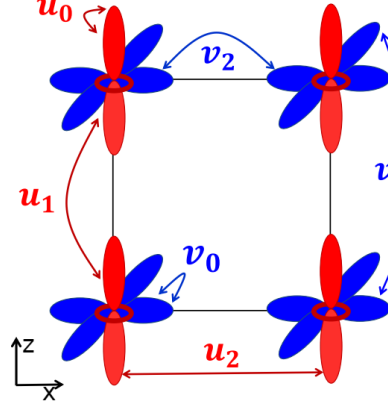


Figure 9. The real space superconducting pairing components up to translation and C_{4v} symmetries.

Table III. Primary superconducting pairing components of LPNO film for $(U, J_H) = (3, 0.3)$ eV and $n = 1.25$ under different in-plane lattice constant compression ratios.

	u_0	u_1	u_2	v_0	v_1	v_2
$\epsilon=2\%, \epsilon_c=1\%$	-0.29303	0.37294	-0.20121	0.25676	0.04816	-0.02430
$\epsilon=3\%, \epsilon_c=1.5\%$	-0.33226	0.54933	-0.12252	0.12190	0.03447	-0.01098
$\epsilon=4\%, \epsilon_c=2\%$	-0.32034	0.58982	-0.09699	0.07555	0.02647	-0.00572
$\epsilon=5\%, \epsilon_c=2.5\%$	-0.28334	0.61586	-0.09119	0.05027	0.02067	-0.00317

Table IV. Primary superconducting pairing components of LNO film for $(U, J_H) = (3, 0.3)$ eV and $n = 1.25$ under different in-plane lattice constant compression ratios.

	u_0	u_1	u_2	v_0	v_1	v_2
$\epsilon=3\%, \epsilon_c=0\%$	-0.31397	0.37124	-0.18666	0.27428	0.04246	-0.02536
$\epsilon=4\%, \epsilon_c=0\%$	-0.34858	0.52732	-0.12570	0.14490	0.03289	-0.01283
$\epsilon=5\%, \epsilon_c=0\%$	-0.34505	0.57133	-0.09825	0.09160	0.02659	-0.00707

* These authors contributed equally to this work.

[†] Contact author: hylu@qfnu.edu.cn

[‡] Contact author: dawang@nju.edu.cn

[§] Contact author: qhwang@nju.edu.cn

[1] H. Sun, M. Huo, X. Hu, J. Li, Z. Liu, Y. Han, L. Tang,

- Z. Mao, P. Yang, B. Wang, J. Cheng, D.-X. Yao, G.-M. Zhang, and M. Wang, Signatures of superconductivity near 80 K in a nickelate under high pressure, *Nature* **621**, 493 (2023).
- [2] Y. Zhu, D. Peng, E. Zhang, B. Pan, X. Chen, L. Chen, H. Ren, F. Liu, Y. Hao, N. Li, Z. Xing, F. Lan, J. Han, J. Wang, D. Jia, H. Wo, Y. Gu, Y. Gu, L. Ji, W. Wang, H. Gou, Y. Shen, T. Ying, X. Chen, W. Yang, H. Cao, C. Zheng, Q. Zeng, J.-g. Guo, and J. Zhao, Superconductivity in pressurized trilayer $\text{La}_3\text{Ni}_4\text{O}_{10-\delta}$ single crystals, *Nature* **631**, 531 (2024).
- [3] Q. Li, Y.-J. Zhang, Z.-N. Xiang, Y. Zhang, X. Zhu, and H.-H. Wen, Signature of superconductivity in pressurized $\text{La}_3\text{Ni}_4\text{O}_{10}$, *Chin. Phys. Lett.* **41**, 017401 (2024).
- [4] X. Chen, J. Choi, Z. Jiang, J. Mei, K. Jiang, J. Li, S. Agrestini, M. Garcia-Fernandez, H. Sun, X. Huang, D. Shen, M. Wang, J. Hu, Y. Lu, K.-J. Zhou, and D. Feng, Electronic and magnetic excitations in $\text{La}_3\text{Ni}_2\text{O}_7$, *Nat. Commun.* **15**, 9597 (2024).
- [5] Z. Liu, M. Huo, J. Li, Q. Li, Y. Liu, Y. Dai, X. Zhou, J. Hao, Y. Lu, M. Wang, and H.-H. Wen, Electronic correlations and partial gap in the bilayer nickelate $\text{La}_3\text{Ni}_2\text{O}_7$, *Nat. Commun.* **15**, 7570 (2024).
- [6] S. Cai, Y. Zhou, H. Sun, K. Zhang, J. Zhao, M. Huo, L. Nataf, Y. Wang, J. Li, J. Guo, K. Jiang, M. Wang, Y. Ding, W. Yang, Y. Lu, Q. Kong, Q. Wu, J. Hu, T. Xiang, H.-k. Mao, and L. Sun, Low-temperature mean valence of nickel ions in pressurized $\text{La}_3\text{Ni}_2\text{O}_7$, *Phys. Rev. B* **111**, 104511 (2025).
- [7] Y. Li, Y. Cao, L. Liu, P. Peng, H. Lin, C. Pei, M. Zhang, H. Wu, X. Du, W. Zhao, K. Zhai, X. Zhang, J. Zhao, M. Lin, P. Tan, Y. Qi, G. Li, H. Guo, L. Yang, and L. Yang, Distinct ultrafast dynamics of bilayer and trilayer nickelate superconductors regarding the density-wave-like transitions, *Sci. Bull.* **70**, 180 (2025).
- [8] J. Hou, P.-T. Yang, Z.-Y. Liu, J.-Y. Li, P.-F. Shan, L. Ma, G. Wang, N.-N. Wang, H.-Z. Guo, J.-P. Sun, Y. Uwatoko, M. Wang, G.-M. Zhang, B.-S. Wang, and J.-G. Cheng, Emergence of high-temperature superconducting phase in pressurized $\text{La}_3\text{Ni}_2\text{O}_7$ crystals, *Chin. Phys. Lett.* **40**, 117302 (2023).
- [9] Y. Zhang, D. Su, Y. Huang, Z. Shan, H. Sun, M. Huo, K. Ye, J. Zhang, Z. Yang, Y. Xu, Y. Su, R. Li, M. Smidman, M. Wang, L. Jiao, and H. Yuan, High-temperature superconductivity with zero resistance and strange-metal behaviour in $\text{La}_3\text{Ni}_2\text{O}_{7-\delta}$, *Nature Physics* **20**, 1269 (2024).
- [10] M. Zhang, C. Pei, Q. Wang, Y. Zhao, C. Li, W. Cao, S. Zhu, J. Wu, and Y. Qi, Effects of pressure and doping on Ruddlesden-Popper phases $\text{La}_{n+1}\text{Ni}_n\text{O}_{3n+1}$, *J. Mater. Sci. Technol.* **185**, 147 (2024).
- [11] N. Wang, G. Wang, X. Shen, J. Hou, J. Luo, X. Ma, H. Yang, L. Shi, J. Dou, J. Feng, J. Yang, Y. Shi, Z. Ren, H. Ma, P. Yang, Z. Liu, Y. Liu, H. Zhang, X. Dong, Y. Wang, K. Jiang, J. Hu, S. Nagasaki, K. Kitagawa, S. Calder, J. Yan, J. Sun, B. Wang, R. Zhou, Y. Uwatoko, and J. Cheng, Bulk high-temperature superconductivity in pressurized tetragonal $\text{La}_2\text{PrNi}_2\text{O}_7$, *Nature* **634**, 579 (2024).
- [12] L. Wang, Y. Li, S.-Y. Xie, F. Liu, H. Sun, C. Huang, Y. Gao, T. Nakagawa, B. Fu, B. Dong, Z. Cao, R. Yu, S. I. Kawaguchi, H. Kadobayashi, M. Wang, C. Jin, H.-k. Mao, and H. Liu, Structure responsible for the superconducting state in $\text{La}_3\text{Ni}_2\text{O}_7$ at high-pressure and low-temperature conditions, *J. Am. Chem. Soc.* **146**, 7506 (2024).
- [13] Y. Zhou, J. Guo, S. Cai, H. Sun, C. Li, J. Zhao, P. Wang, J. Han, X. Chen, Y. Chen, Q. Wu, Y. Ding, T. Xiang, H.-k. Mao, and L. Sun, Investigations of key issues on the reproducibility of high- T_c superconductivity emerging from compressed $\text{La}_3\text{Ni}_2\text{O}_7$, *Matter Radiat. Extremes* **10**, 027801 (2025).
- [14] T. Cui, S. Choi, T. Lin, C. Liu, G. Wang, N. Wang, S. Chen, H. Hong, D. Rong, Q. Wang, Q. Jin, J.-O. Wang, L. Gu, C. Ge, C. Wang, J.-G. Cheng, Q. Zhang, L. Si, K.-j. Jin, and E.-J. Guo, Strain-mediated phase crossover in Ruddlesden-Popper nickelates, *Commun. Mater.* **5**, 32 (2024).
- [15] K. Chen, X. Liu, J. Jiao, M. Zou, C. Jiang, X. Li, Y. Luo, Q. Wu, N. Zhang, Y. Guo, and L. Shu, Evidence of spin density waves in $\text{La}_3\text{Ni}_2\text{O}_{7-\delta}$, *Phys. Rev. Lett.* **132**, 256503 (2024).
- [16] X. Chen, J. Zhang, A. S. Thind, S. Sharma, H. LaBolita, G. Peterson, H. Zheng, D. P. Phelan, A. S. Botana, R. F. Klie, and J. F. Mitchell, Polymorphism in the Ruddlesden-Popper nickelate $\text{La}_3\text{Ni}_2\text{O}_7$: Discovery of a hidden phase with distinctive layer stacking, *J. Am. Chem. Soc.* **146**, 3640 (2024).
- [17] P. Puphal, P. Reiss, N. Enderlein, Y.-M. Wu, G. Khalilullin, V. Sundaramurthy, T. Priessnitz, M. Knauft, A. Suthar, L. Richter, M. Isobe, P. A. van Aken, H. Takagi, B. Keimer, Y. E. Suyolcu, B. Wehinger, P. Hansmann, and M. Hepting, Unconventional crystal structure of the high-pressure superconductor $\text{La}_3\text{Ni}_2\text{O}_7$, *Phys. Rev. Lett.* **133**, 146002 (2024).
- [18] H. Wang, L. Chen, A. Rutherford, H. Zhou, and W. Xie, Long-range structural order in a hidden phase of Ruddlesden-Popper bilayer nickelate $\text{La}_3\text{Ni}_2\text{O}_7$, *Inorg. Chem.* **63**, 5020 (2024).
- [19] M. Kakoi, T. Oi, Y. Ohshita, M. Yashima, K. Kuroki, T. Kato, H. Takahashi, S. Ishiwata, Y. Adachi, N. Hatada, T. Uda, and H. Mukuda, Multiband metallic ground state in multilayered nickelates $\text{La}_3\text{Ni}_2\text{O}_7$ and $\text{La}_4\text{Ni}_3\text{O}_{10}$ probed by ^{139}La -NMR at ambient pressure, *J. Phys. Soc. Jpn.* **93**, 053702 (2024).
- [20] M. Xu, S. Huyan, H. Wang, S. L. Bud'ko, X. Chen, X. Ke, J. F. Mitchell, P. C. Canfield, J. Li, and W. Xie, Pressure-dependent “insulator–metal–insulator” behavior in Sr-doped $\text{La}_3\text{Ni}_2\text{O}_7$, *Adv. Electron. Mater.* **10**, 2400078 (2024).
- [21] Z. Dong, M. Huo, J. Li, J. Li, P. Li, H. Sun, L. Gu, Y. Lu, M. Wang, Y. Wang, and Z. Chen, Visualization of oxygen vacancies and self-doped ligand holes in $\text{La}_3\text{Ni}_2\text{O}_{7-\delta}$, *Nature* **630**, 847 (2024).
- [22] E. Talantsev and V. Chistyakov, Debye temperature, electron-phonon coupling constant, and three-dome shape of crystalline strain as a function of pressure in highly compressed $\text{La}_3\text{Ni}_2\text{O}_{7-\delta}$, *Lett. Mater.* **14**, 262 (2024).
- [23] B. Geisler, L. Fanfarillo, J. J. Hamlin, G. R. Stewart, R. G. Hennig, and P. J. Hirschfeld, Optical properties and electronic correlations in $\text{La}_3\text{Ni}_2\text{O}_7$ bilayer nickelates under high pressure, *npj Quantum Mater.* **9**, 89 (2024).
- [24] J. Yang, H. Sun, X. Hu, Y. Xie, T. Miao, H. Luo, H. Chen, B. Liang, W. Zhu, G. Qu, C.-Q. Chen, M. Huo, Y. Huang, S. Zhang, F. Zhang, F. Yang, Z. Wang, Q. Peng, H. Mao, G. Liu, Z. Xu, T. Qian, D.-X. Yao,

- M. Wang, L. Zhao, and X. J. Zhou, Orbital-dependent electron correlation in double-layer nickelate $\text{La}_3\text{Ni}_2\text{O}_7$, *Nat. Commun.* **15**, 4373 (2024).
- [25] D. Takegami, K. Fujinuma, R. Nakamura, M. Yoshimura, K.-D. Tsuei, G. Wang, N. N. Wang, J.-G. Cheng, Y. Uwatoko, and T. Mizokawa, Absence of $\text{Ni}^{2+}/\text{Ni}^{3+}$ charge disproportionation and possible roles of O 2p holes in $\text{La}_3\text{Ni}_2\text{O}_{7-\delta}$ revealed by hard x-ray photoemission spectroscopy, *Phys. Rev. B* **109**, 125119 (2024).
- [26] G. Wang, N. N. Wang, X. L. Shen, J. Hou, L. Ma, L. F. Shi, Z. A. Ren, Y. D. Gu, H. M. Ma, P. T. Yang, Z. Y. Liu, H. Z. Guo, J. P. Sun, G. M. Zhang, S. Calder, J.-Q. Yan, B. S. Wang, Y. Uwatoko, and J.-G. Cheng, Pressure-induced superconductivity in polycrystalline $\text{La}_3\text{Ni}_2\text{O}_{7-\delta}$, *Phys. Rev. X* **14**, 011040 (2024).
- [27] J. Li, D. Peng, P. Ma, H. Zhang, Z. Xing, X. Huang, C. Huang, M. Huo, D. Hu, Z. Dong, X. Chen, T. Xie, H. Dong, H. Sun, Q. Zeng, H.-k. Mao, and M. Wang, Identification of superconductivity in bilayer nickelate $\text{La}_3\text{Ni}_2\text{O}_7$ under high pressure up to 100 GPa, *Natl. Sci. Rev.*, nwaf220 (2025).
- [28] M. Shi, Y. Li, Y. Wang, D. Peng, S. Yang, H. Li, K. Fan, K. Jiang, J. He, Q. Zeng, D. Song, B. Ge, Z. Xiang, Z. Wang, J. Ying, T. Wu, and X. Chen, Absence of superconductivity and density-wave transition in ambient-pressure tetragonal $\text{La}_4\text{Ni}_3\text{O}_{10}$, *Nat. Commun.* **16**, 2887 (2025).
- [29] R. Khasanov, I. Plokhikh, T. J. Hicken, H. Luetkens, D. J. Gawryluk, and Z. Guguchia, Pressure effect on the spin density wave transition in $\text{La}_2\text{PrNi}_2\text{O}_{6.96}$, *Phys. Rev. Res.* **7**, L022046 (2025).
- [30] S. F. R. TenHuisen, G. A. Pan, Q. Song, D. R. Baykushova, D. Ferenc Segedin, B. H. Goodge, H. Paik, J. Pelliciari, V. Bisogni, Y. Gu, S. Agrestini, A. Nag, M. García-Fernández, K.-J. Zhou, L. F. Kourkoutis, C. M. Brooks, J. A. Mundy, M. P. M. Dean, and M. Mitrano, Magnetic excitations in $\text{Nd}_{n+1}\text{Ni}_n\text{O}_{3n+1}$ ruddlesden-popper nickelates observed via resonant inelastic x-ray scattering, *Phys. Rev. B* **111**, 165145 (2025).
- [31] Y. Meng, Y. Yang, H. Sun, S. Zhang, J. Luo, L. Chen, X. Ma, M. Wang, F. Hong, X. Wang, and X. Yu, Density-wave-like gap evolution in $\text{La}_3\text{Ni}_2\text{O}_7$ under high pressure revealed by ultrafast optical spectroscopy, *Nat. Commun.* **15**, 10408 (2024).
- [32] M. Shi, D. Peng, Y. Li, Z. Xing, Y. Wang, K. Fan, H. Li, R. Wu, Z. Zeng, Q. Zeng, J. Ying, T. Wu, and X. Chen, Prerequisite of superconductivity: SDW rather than tetragonal structure in double-layer $\text{La}_3\text{Ni}_2\text{O}_{7-x}$ (2025), arXiv:2501.14202 [cond-mat.supr-con].
- [33] D. Zhao, Y. Zhou, M. Huo, Y. Wang, L. Nie, Y. Yang, J. Ying, M. Wang, T. Wu, and X. Chen, Pressure-enhanced spin-density-wave transition in double-layer nickelate $\text{La}_3\text{Ni}_2\text{O}_{7-\delta}$, *Sci. Bull.* **70**, 1239 (2025).
- [34] G. Wang, N. Wang, T. Lu, S. Calder, J. Yan, L. Shi, J. Hou, L. Ma, L. Zhang, J. Sun, B. Wang, S. Meng, M. Liu, and J. Cheng, Chemical versus physical pressure effects on the structure transition of bilayer nickelates, *npj Quantum Mater.* **10**, 1 (2025).
- [35] M. Zhang, C. Pei, D. Peng, X. Du, W. Hu, Y. Cao, Q. Wang, J. Wu, Y. Li, H. Liu, C. Wen, J. Song, Y. Zhao, C. Li, W. Cao, S. Zhu, Q. Zhang, N. Yu, P. Cheng, L. Zhang, Z. Li, J. Zhao, Y. Chen, C. Jin, H. Guo, C. Wu, F. Yang, Q. Zeng, S. Yan, L. Yang, and Y. Qi, Superconductivity in trilayer nickelate $\text{La}_4\text{Ni}_3\text{O}_{10}$ under pressure, *Phys. Rev. X* **15**, 021005 (2025).
- [36] Y. Chen, K. Zhang, M. Xu, Y. Zhao, H. Xiao, and L. Qiao, Oxygen deficiency mechanism of $\text{La}_3\text{Ni}_2\text{O}_{7-\delta}$ under pressure, *Sci. China-Phys. Mech. Astron.* **68**, 247411 (2025).
- [37] S. Abadi, K.-J. Xu, E. G. Lomeli, P. Puphal, M. Isobe, Y. Zhong, A. V. Fedorov, S.-K. Mo, M. Hashimoto, D.-H. Lu, B. Moritz, B. Keimer, T. P. Devereaux, M. Hepting, and Z.-X. Shen, Electronic structure of the alternating monolayer-trilayer phase of $\text{La}_3\text{Ni}_2\text{O}_7$, *Phys. Rev. Lett.* **134**, 126001 (2025).
- [38] S. Xu, H. Wang, M. Huo, D. Hu, Q. Wu, L. Yue, D. Wu, M. Wang, T. Dong, and N. Wang, Collapse of density wave and emergence of superconductivity in pressurized- $\text{La}_4\text{Ni}_3\text{O}_{10}$ evidenced by ultrafast spectroscopy (2025), arXiv:2503.05176 [cond-mat.supr-con].
- [39] C. Liu, M. Huo, H. Yang, Q. Li, Y. Zhang, Z. Xiang, M. Wang, and H.-H. Wen, Andreev reflection in superconducting state of pressurized $\text{La}_3\text{Ni}_2\text{O}_7$, *Sci. China-Phys. Mech. Astron.* **68**, 247412 (2025).
- [40] F. Li, Z. Xing, D. Peng, J. Dou, N. Guo, L. Ma, Y. Zhang, L. Wang, J. Luo, J. Yang, J. Zhang, T. Chang, Y.-S. Chen, W. Cai, J. Cheng, Y. Wang, Z. Zeng, Q. Zheng, R. Zhou, Q. Zeng, X. Tao, and J. Zhang, Ambient pressure growth of bilayer nickelate single crystals with superconductivity over 90 K under high pressure (2025), arXiv:2501.14584 [cond-mat.supr-con].
- [41] E. Zhang, D. Peng, Y. Zhu, L. Chen, B. Cui, X. Wang, W. Wang, Q. Zeng, and J. Zhao, Bulk superconductivity in pressurized trilayer nickelate $\text{Pr}_4\text{Ni}_3\text{O}_{10}$ single crystals, *Phys. Rev. X* **15**, 021008 (2025).
- [42] M. Wang, H.-H. Wen, T. Wu, D.-X. Yao, and T. Xiang, Normal and superconducting properties of $\text{La}_3\text{Ni}_2\text{O}_7$, *Chin. Phys. Lett.* **41**, 077402 (2024).
- [43] Z. Luo, X. Hu, M. Wang, W. Wú, and D.-X. Yao, Bilayer two-orbital model of $\text{La}_3\text{Ni}_2\text{O}_7$ under pressure, *Phys. Rev. Lett.* **131**, 126001 (2023).
- [44] Q.-G. Yang, D. Wang, and Q.-H. Wang, Possible s_{\pm} -wave superconductivity in $\text{La}_3\text{Ni}_2\text{O}_7$, *Phys. Rev. B* **108**, L140505 (2023).
- [45] Y. Zhang, L.-F. Lin, A. Moreo, and E. Dagotto, Electronic structure, dimer physics, orbital-selective behavior, and magnetic tendencies in the bilayer nickelate superconductor $\text{La}_3\text{Ni}_2\text{O}_7$ under pressure, *Phys. Rev. B* **108**, L180510 (2023).
- [46] H. Sakakibara, N. Kitamine, M. Ochi, and K. Kuroki, Possible high T_c superconductivity in $\text{La}_3\text{Ni}_2\text{O}_7$ under high pressure through manifestation of a nearly half-filled bilayer Hubbard model, *Phys. Rev. Lett.* **132**, 106002 (2024).
- [47] Y. Gu, C. Le, Z. Yang, X. Wu, and J. Hu, Effective model and pairing tendency in the bilayer Ni-based superconductor $\text{La}_3\text{Ni}_2\text{O}_7$, *Phys. Rev. B* **111**, 174506 (2025).
- [48] V. Christiansson, F. Petocchi, and P. Werner, Correlated electronic structure of $\text{La}_3\text{Ni}_2\text{O}_7$ under pressure, *Phys. Rev. Lett.* **131**, 206501 (2023).
- [49] D. A. Shilenko and I. V. Leonov, Correlated electronic structure, orbital-selective behavior, and magnetic correlations in double-layer $\text{La}_3\text{Ni}_2\text{O}_7$ under pressure, *Phys. Rev. B* **108**, 125105 (2023).

- [50] T. Kaneko, H. Sakakibara, M. Ochi, and K. Kuroki, Pair correlations in the two-orbital Hubbard ladder: Implications for superconductivity in the bilayer nickelate $\text{La}_3\text{Ni}_2\text{O}_7$, *Phys. Rev. B* **109**, 045154 (2024).
- [51] Y. Shen, M. Qin, and G.-M. Zhang, Effective bi-layer model Hamiltonian and density-matrix renormalization group study for the high- T_c superconductivity in $\text{La}_3\text{Ni}_2\text{O}_7$ under high pressure, *Chin. Phys. Lett.* **40**, 127401 (2023).
- [52] W. Wú, Z. Luo, D.-X. Yao, and M. Wang, Superexchange and charge transfer in the nickelate superconductor $\text{La}_3\text{Ni}_2\text{O}_7$ under pressure, *Sci. China-Phys. Mech. Astron.* **67**, 117402 (2024).
- [53] Y. Cao and Y.-f. Yang, Flat bands promoted by Hund's rule coupling in the candidate double-layer high-temperature superconductor $\text{La}_3\text{Ni}_2\text{O}_7$ under high pressure, *Phys. Rev. B* **109**, L081105 (2024).
- [54] X. Chen, P. Jiang, J. Li, Z. Zhong, and Y. Lu, Charge and spin instabilities in superconducting $\text{La}_3\text{Ni}_2\text{O}_7$, *Phys. Rev. B* **111**, 014515 (2025).
- [55] J. Chen, F. Yang, and W. Li, Orbital-selective superconductivity in the pressurized bilayer nickelate $\text{La}_3\text{Ni}_2\text{O}_7$: An infinite projected entangled-pair state study, *Phys. Rev. B* **110**, L041111 (2024).
- [56] Y.-B. Liu, J.-W. Mei, F. Ye, W.-Q. Chen, and F. Yang, s_{\pm} -wave pairing and the destructive role of apical-oxygen deficiencies in $\text{La}_3\text{Ni}_2\text{O}_7$ under pressure, *Phys. Rev. Lett.* **131**, 236002 (2023).
- [57] C. Lu, Z. Pan, F. Yang, and C. Wu, Interlayer-coupling-driven high-temperature superconductivity in $\text{La}_3\text{Ni}_2\text{O}_7$ under pressure, *Phys. Rev. Lett.* **132**, 146002 (2024).
- [58] Z. Ouyang, M. Gao, and Z.-Y. Lu, Absence of electron-phonon coupling superconductivity in the bilayer phase of $\text{La}_3\text{Ni}_2\text{O}_7$ under pressure, *npj Quantum Mater.* **9**, 80 (2024).
- [59] Y. Zhang, L.-F. Lin, A. Moreo, T. A. Maier, and E. Dagotto, Structural phase transition, s_{\pm} -wave pairing, and magnetic stripe order in bilayered superconductor $\text{La}_3\text{Ni}_2\text{O}_7$ under pressure, *Nat. Commun.* **15**, 2470 (2024).
- [60] X.-W. Yi, Y. Meng, J.-W. Li, Z.-W. Liao, W. Li, J.-Y. You, B. Gu, and G. Su, Nature of charge density waves and metal-insulator transition in pressurized $\text{La}_3\text{Ni}_2\text{O}_7$, *Phys. Rev. B* **110**, L140508 (2024).
- [61] H. Oh and Y.-H. Zhang, Type-II $t-J$ model and shared superexchange coupling from Hund's rule in superconducting $\text{La}_3\text{Ni}_2\text{O}_7$, *Phys. Rev. B* **108**, 174511 (2023).
- [62] X.-Z. Qu, D.-W. Qu, J. Chen, C. Wu, F. Yang, W. Li, and G. Su, Bilayer $t-J-J_{\perp}$ model and magnetically mediated pairing in the pressurized nickelate $\text{La}_3\text{Ni}_2\text{O}_7$, *Phys. Rev. Lett.* **132**, 036502 (2024).
- [63] Y.-f. Yang, G.-M. Zhang, and F.-C. Zhang, Interlayer valence bonds and two-component theory for high- T_c superconductivity of $\text{La}_3\text{Ni}_2\text{O}_7$ under pressure, *Phys. Rev. B* **108**, L201108 (2023).
- [64] F. Lechermann, J. Gondolf, S. Böttzel, and I. M. Eremin, Electronic correlations and superconducting instability in $\text{La}_3\text{Ni}_2\text{O}_7$ under high pressure, *Phys. Rev. B* **108**, L201121 (2023).
- [65] Z. Liao, L. Chen, G. Duan, Y. Wang, C. Liu, R. Yu, and Q. Si, Electron correlations and superconductivity in $\text{La}_3\text{Ni}_2\text{O}_7$ under pressure tuning, *Phys. Rev. B* **108**, 214522 (2023).
- [66] K. Jiang, Z. Wang, and F.-C. Zhang, High-temperature superconductivity in $\text{La}_3\text{Ni}_2\text{O}_7$, *Chin. Phys. Lett.* **41**, 017402 (2024).
- [67] J.-X. Zhang, H.-K. Zhang, Y.-Z. You, and Z.-Y. Weng, Strong pairing originated from an emergent Z_2 berry phase in $\text{La}_3\text{Ni}_2\text{O}_7$, *Phys. Rev. Lett.* **133**, 126501 (2024).
- [68] C. Lu, Z. Pan, F. Yang, and C. Wu, Interplay of two E_g orbitals in superconducting $\text{La}_3\text{Ni}_2\text{O}_7$ under pressure, *Phys. Rev. B* **110**, 094509 (2024).
- [69] J. Huang and T. Zhou, Interlayer pairing-induced partially gapped fermi surface in trilayer $\text{La}_4\text{Ni}_3\text{O}_{10}$ superconductors, *Phys. Rev. B* **110**, L060506 (2024).
- [70] C. Xia, H. Liu, S. Zhou, and H. Chen, Sensitive dependence of pairing symmetry on $\text{Ni}-e_g$ crystal field splitting in the nickelate superconductor $\text{La}_3\text{Ni}_2\text{O}_7$, *Nat. Commun.* **16**, 1054 (2025).
- [71] G. Heier, K. Park, and S. Y. Savrasov, Competing d_{xy} and s_{\pm} pairing symmetries in superconducting $\text{La}_3\text{Ni}_2\text{O}_7$: LDA + FLEX calculations, *Phys. Rev. B* **109**, 104508 (2024).
- [72] Z. Luo, B. Lv, M. Wang, W. Wú, and D.-X. Yao, High- t_c superconductivity in $\text{La}_3\text{Ni}_2\text{O}_7$ based on the bi-layer two-orbital t-J model, *npj Quantum Mater.* **9**, 61 (2024).
- [73] J. Huang, Z. D. Wang, and T. Zhou, Impurity and vortex states in the bilayer high-temperature superconductor $\text{La}_3\text{Ni}_2\text{O}_7$, *Phys. Rev. B* **108**, 174501 (2023).
- [74] Y. Zhang, L.-F. Lin, A. Moreo, T. A. Maier, and E. Dagotto, Trends in electronic structures and s_{\pm} -wave pairing for the rare-earth series in bilayer nickelate superconductor $R_3\text{Ni}_2\text{O}_7$, *Phys. Rev. B* **108**, 165141 (2023).
- [75] Y.-H. Tian, Y. Chen, J.-M. Wang, R.-Q. He, and Z.-Y. Lu, Correlation effects and concomitant two-orbital s_{\pm} -wave superconductivity in $\text{La}_3\text{Ni}_2\text{O}_7$ under high pressure, *Phys. Rev. B* **109**, 165154 (2024).
- [76] Q. Qin and Y.-F. Yang, High- T_c superconductivity by mobilizing local spin singlets and possible route to higher T_c in pressurized $\text{La}_3\text{Ni}_2\text{O}_7$, *Phys. Rev. B* **108**, L140504 (2023).
- [77] S. Ryee, N. Witt, and T. O. Wehling, Quenched pair breaking by interlayer correlations as a key to superconductivity in $\text{La}_3\text{Ni}_2\text{O}_7$, *Phys. Rev. Lett.* **133**, 096002 (2024).
- [78] Z. Ouyang, J.-M. Wang, J.-X. Wang, R.-Q. He, L. Huang, and Z.-Y. Lu, Hund electronic correlation in $\text{La}_3\text{Ni}_2\text{O}_7$ under high pressure, *Phys. Rev. B* **109**, 115114 (2024).
- [79] X.-Z. Qu, D.-W. Qu, X.-W. Yi, W. Li, and G. Su, Hund's rule, interorbital hybridization, and high- T_c superconductivity in the bilayer nickelate (2025), arXiv:2311.12769 [cond-mat.str-el].
- [80] Y.-Y. Zheng and W. Wú, s_{\pm} -wave superconductivity in the bilayer two-orbital Hubbard model, *Phys. Rev. B* **111**, 035108 (2025).
- [81] M. Kakoi, T. Kaneko, H. Sakakibara, M. Ochi, and K. Kuroki, Pair correlations of the hybridized orbitals in a ladder model for the bilayer nickelate $\text{La}_3\text{Ni}_2\text{O}_7$, *Phys. Rev. B* **109**, L201124 (2024).
- [82] Z. Fan, J.-F. Zhang, B. Zhan, D. Lv, X.-Y. Jiang, B. Normand, and T. Xiang, Superconductivity in nickelate and cuprate superconductors with strong bilayer coupling, *Phys. Rev. B* **110**, 024514 (2024).
- [83] Y. Wang, K. Jiang, Z. Wang, F.-C. Zhang, and J. Hu,

- Electronic and magnetic structures of bilayer $\text{La}_3\text{Ni}_2\text{O}_7$ at ambient pressure, *Phys. Rev. B* **110**, 205122 (2024).
- [84] S. Bötzel, F. Lechermann, J. Gondolf, and I. M. Eremin, Theory of magnetic excitations in the multilayer nickelate superconductor $\text{La}_3\text{Ni}_2\text{O}_7$, *Phys. Rev. B* **109**, L180502 (2024).
- [85] J.-R. Xue and F. Wang, Magnetism and superconductivity in the t - J model of $\text{La}_3\text{Ni}_2\text{O}_7$ under multiband Gutzwiller approximation, *Chin. Phys. Lett.* **41**, 057403 (2024).
- [86] B. Geisler, J. J. Hamlin, G. R. Stewart, R. G. Henning, and P. J. Hirschfeld, Structural transitions, octahedral rotations, and electronic properties of $A_3\text{Ni}_2\text{O}_7$ rare-earth nickelates under high pressure, *npj Quantum Mater.* **9**, 38 (2024).
- [87] L. C. Rhodes and P. Wahl, Structural routes to stabilize superconducting $\text{La}_3\text{Ni}_2\text{O}_7$ at ambient pressure, *Phys. Rev. Mater.* **8**, 044801 (2024).
- [88] L. Craco and S. Leoni, Strange metal and coherence-incoherence crossover in pressurized $\text{La}_3\text{Ni}_2\text{O}_7$, *Phys. Rev. B* **109**, 165116 (2024).
- [89] R. Jiang, J. Hou, Z. Fan, Z.-J. Lang, and W. Ku, Pressure driven fractionalization of ionic spins results in cupratelike high- T_c superconductivity in $\text{La}_3\text{Ni}_2\text{O}_7$, *Phys. Rev. Lett.* **132**, 126503 (2024).
- [90] H. Lange, L. Homeier, E. Demler, U. Schollwöck, F. Grusdt, and A. Bohrdt, Feshbach resonance in a strongly repulsive ladder of mixed dimensionality: A possible scenario for bilayer nickelate superconductors, *Phys. Rev. B* **109**, 045127 (2024).
- [91] Z. Huo, Z. Luo, P. Zhang, A. Yang, Z. Liu, X. Tao, Z. Zhang, S. Guo, Q. Jiang, W. Chen, D.-X. Yao, D. Duan, and T. Cui, Modulation of the octahedral structure and potential superconductivity of $\text{La}_3\text{Ni}_2\text{O}_7$ through strain engineering, *Sci. China-Phys. Mech. Astron.* **68**, 237411 (2025).
- [92] S. Bötzel, F. Lechermann, T. Shibauchi, and I. M. Eremin, Theory of potential impurity scattering in pressurized superconducting $\text{La}_3\text{Ni}_2\text{O}_7$, *Commun. Phys.* **8**, 154 (2025).
- [93] J.-Y. You, Z. Zhu, M. Del Ben, W. Chen, and Z. Li, Unlikelihood of a phonon mechanism for the high-temperature superconductivity in $\text{La}_3\text{Ni}_2\text{O}_7$, *npj Comput. Mater.* **11**, 3 (2025).
- [94] C. Zhu, B. Li, Y. Fan, C. Yin, J. Zhai, J. Cheng, S. Liu, and Z. Shi, Magnetic phases and electron-phonon coupling in $\text{La}_3\text{Ni}_2\text{O}_7$ under pressure, *Comput. Mater. Sci.* **250**, 113676 (2025).
- [95] Z. Huo, P. Zhang, H. Shi, X. Yan, D. Duan, and T. Cui, First-principles study of the Pr-doped bilayer nickelate $\text{La}_3\text{Ni}_2\text{O}_7$, *Phys. Rev. B* **111**, 195118 (2025).
- [96] W. Xi, S.-L. Yu, and J.-X. Li, Transition from s_{\pm} -wave to $d_{x^2-y^2}$ -wave superconductivity driven by interlayer interaction in the bilayer two-orbital model of $\text{La}_3\text{Ni}_2\text{O}_7$, *Phys. Rev. B* **111**, 104505 (2025).
- [97] J. Zhan, Y. Gu, X. Wu, and J. Hu, Cooperation between electron-phonon coupling and electronic interaction in bilayer nickelates $\text{La}_3\text{Ni}_2\text{O}_7$, *Phys. Rev. Lett.* **134**, 136002 (2025).
- [98] J. Zhan, C. Le, X. Wu, and J. Hu, Impact of nonlocal coulomb repulsion on superconductivity and density-wave orders in bilayer nickelates (2025), arXiv:2503.18877 [cond-mat.supr-con].
- [99] C. Lu, M. Zhang, Z. Pan, C. Wu, and F. Yang, Impact of pressure and apical oxygen vacancies on superconductivity in $\text{La}_3\text{Ni}_2\text{O}_7$ (2025), arXiv:2502.14324 [cond-mat.supr-con].
- [100] J.-H. Ji, C. Lu, Z.-Y. Shao, Z. Pan, F. Yang, and C. Wu, A strong-coupling-limit study on the pairing mechanism in the pressurized $\text{La}_3\text{Ni}_2\text{O}_7$ (2025), arXiv:2504.12127 [cond-mat.supr-con].
- [101] M. Zhang, H. Sun, Y.-B. Liu, Q. Liu, W.-Q. Chen, and F. Yang, s^{\pm} -wave superconductivity in pressurized $\text{La}_4\text{Ni}_3\text{O}_{10}$, *Phys. Rev. B* **110**, L180501 (2024).
- [102] Y.-Q. Liu, D. Wang, and Q.-H. Wang, Variational quantum monte carlo investigations of the superconducting pairing in $\text{La}_3\text{Ni}_2\text{O}_7$ (2025), arXiv:2505.07341 [cond-mat.supr-con].
- [103] E. K. Ko, Y. Yu, Y. Liu, L. Bhatt, J. Li, V. Thampy, C.-T. Kuo, B. Y. Wang, Y. Lee, K. Lee, J.-S. Lee, B. H. Goodge, D. A. Muller, and H. Y. Hwang, Signatures of ambient pressure superconductivity in thin film $\text{La}_3\text{Ni}_2\text{O}_7$, *Nature* **638**, 935 (2025).
- [104] G. Zhou, W. Lv, H. Wang, Z. Nie, Y. Chen, Y. Li, H. Huang, W.-Q. Chen, Y.-J. Sun, Q.-K. Xue, and Z. Chen, Ambient-pressure superconductivity onset above 40 K in $(\text{La},\text{Pr})_3\text{Ni}_2\text{O}_7$, *Nature* **640**, 641 (2025).
- [105] L. Bhatt, A. Y. Jiang, E. K. Ko, N. Schnitzer, G. A. Pan, D. F. Segedin, Y. Liu, Y. Yu, Y.-F. Zhao, E. A. Morales, C. M. Brooks, A. S. Botana, H. Y. Hwang, J. A. Mundy, D. A. Muller, and B. H. Goodge, Resolving structural origins for superconductivity in strain-engineered $\text{La}_3\text{Ni}_2\text{O}_7$ thin films (2025), arXiv:2501.08204 [cond-mat.supr-con].
- [106] H. Wang, H. Huang, G. Zhou, W. Lv, C. Yue, L. Xu, X. Wu, Z. Nie, Y. Chen, Y.-J. Sun, W. Chen, H. Yuan, Z. Chen, and Q.-K. Xue, Electronic structures across the superconductor-insulator transition at $\text{La}_{2.85}\text{Pr}_{0.15}\text{Ni}_2\text{O}_7/\text{SrLaAlO}_4$ interfaces (2025), arXiv:2502.18068 [cond-mat.supr-con].
- [107] P. Li, G. Zhou, W. Lv, Y. Li, C. Yue, H. Huang, L. Xu, J. Shen, Y. Miao, W. Song, Z. Nie, Y. Chen, H. Wang, W. Chen, Y. Huang, Z.-H. Chen, T. Qian, J. Lin, J. He, Y.-J. Sun, Z. Chen, and Q.-K. Xue, Angle-resolved photoemission spectroscopy of superconducting $(\text{La},\text{Pr})_3\text{Ni}_2\text{O}_7/\text{SrLaAlO}_4$ heterostructures, *Natl. Sci. Rev.*, nwaf205 (2025).
- [108] Y. Liu, E. K. Ko, Y. Tarn, L. Bhatt, J. Li, V. Thampy, B. H. Goodge, D. A. Muller, S. Raghu, Y. Yu, and H. Y. Hwang, Superconductivity and normal-state transport in compressively strained $\text{La}_3\text{PrNi}_2\text{O}_7$ thin films, *Nature Materials* **10**.1038/s41563-025-02258-y (2025).
- [109] B. Y. Wang, Y. Zhong, S. Abadi, Y. Liu, Y. Yu, X. Zhang, Y.-M. Wu, R. Wang, J. Li, Y. Tarn, E. K. Ko, V. Thampy, M. Hashimoto, D. Lu, Y. S. Lee, T. P. Devreux, C. Jia, H. Y. Hwang, and Z.-X. Shen, Electronic structure of compressively strained thin film $\text{la}_2\text{prni}_2\text{o}_7$ (2025), arXiv:2504.16372 [cond-mat.supr-con].
- [110] J. Shen, Y. Miao, Z. Ou, G. Zhou, Y. Chen, R. Luan, H. Sun, Z. Feng, X. Yong, P. Li, Y. Li, L. Xu, W. Lv, Z. Nie, H. Wang, H. Huang, Y.-J. Sun, Q.-K. Xue, Z. Chen, and J. He, Anomalous energy gap in superconducting $\text{La}_{2.85}\text{Pr}_{0.15}\text{Ni}_2\text{O}_7/\text{SrLaAlO}_4$ heterostructures (2025), arXiv:2502.17831 [cond-mat.supr-con].
- [111] K.-Y. Jiang, Y.-H. Cao, Q.-G. Yang, H.-Y. Lu, and Q.-H. Wang, Theory of pressure dependence of superconductivity in bilayer nickelate $\text{La}_3\text{Ni}_2\text{O}_7$, *Phys. Rev. Lett.* **134**, 076001 (2025).

- [112] See Supplemental Material for details of DFT calculations, comparison of DFT and Wannier band structure, main tight-binding parameters under different in-plane compression ratios ϵ , the SM-FRG flow of LNO film, and the real space superconducting pairing components under different in-plane compression ratios ϵ and $n = 1.25$, which includes Refs. [125–130].
- [113] X.-W. Yi, W. Li, J.-Y. You, B. Gu, and G. Su, *Unifying strain-driven and pressure-driven superconductivity in La₃Ni₂O₇: Suppressed charge/spin density waves and enhanced interlayer coupling* (2025), arXiv:2505.12733 [cond-mat.supr-con].
- [114] K. Ushio, S. Kamiyama, Y. Hoshi, R. Mizuno, M. Ochi, K. Kuroki, and H. Sakakibara, *Theoretical study on ambient pressure superconductivity in La₃Ni₂O₇ thin films : structural analysis, model construction, and robustness of s±-wave pairing* (2025), arXiv:2506.20497 [cond-mat.supr-con].
- [115] H. C. R. B. Bhatta, X. Zhang, Y. Zhong, and C. Jia, *Structural and electronic evolution of bilayer nickelates under biaxial strain* (2025), arXiv:2502.01624 [cond-mat.supr-con].
- [116] S. Ryee, N. Witt, G. Sangiovanni, and T. O. Wehling, *Optimal superconductivity near a Lifshitz transition in strained (La,Pr)₃Ni₂O₇* (2025), arXiv:2506.21480 [cond-mat.supr-con].
- [117] C. Castellani, C. R. Natoli, and J. Ranninger, *Magnetic structure of V₂O₃ in the insulating phase*, Phys. Rev. B **18**, 4945 (1978).
- [118] W.-S. Wang, Y.-Y. Xiang, Q.-H. Wang, F. Wang, F. Yang, and D.-H. Lee, *Functional renormalization group and variational Monte Carlo studies of the electronic instabilities in graphene near 1/4 doping*, Phys. Rev. B **85**, 035414 (2012).
- [119] W.-S. Wang, Z.-Z. Li, Y.-Y. Xiang, and Q.-H. Wang, *Competing electronic orders on kagome lattices at van Hove filling*, Phys. Rev. B **87**, 115135 (2013).
- [120] Q.-K. Tang, L. Yang, D. Wang, F.-C. Zhang, and Q.-H. Wang, *Spin-triplet f-wave pairing in twisted bilayer graphene near 1/4-filling*, Phys. Rev. B **99**, 094521 (2019).
- [121] Q.-G. Yang, D. Wang, and Q.-H. Wang, *Functional renormalization group study of the two-dimensional Su-Schrieffer-Heeger-Hubbard model*, Phys. Rev. B **106**, 245136 (2022).
- [122] Q.-G. Yang, K.-Y. Jiang, D. Wang, H.-Y. Lu, and Q.-H. Wang, *Effective model and s±-wave superconductivity in trilayer nickelate La₄Ni₃O₁₀*, Phys. Rev. B **109**, L220506 (2024).
- [123] Q.-G. Yang, M. Yao, D. Wang, and Q.-H. Wang, *Charge bond order and s-wave superconductivity in the kagome lattice with electron-phonon coupling and electron-electron interaction*, Phys. Rev. B **109**, 075130 (2024).
- [124] W. Kohn and J. M. Luttinger, *New Mechanism for Superconductivity*, Phys. Rev. Lett. **15**, 524 (1965).
- [125] G. Kresse and J. Furthmüller, *Efficient iterative schemes for ab initio total-energy calculations using a plane-wave basis set*, Phys. Rev. B **54**, 11169 (1996).
- [126] P. E. Blöchl, *Projector augmented-wave method*, Phys. Rev. B **50**, 17953 (1994).
- [127] J. P. Perdew, K. Burke, and M. Ernzerhof, *Generalized gradient approximation made simple*, Phys. Rev. Lett. **77**, 3865 (1996).
- [128] N. Marzari and D. Vanderbilt, *Maximally localized generalized Wannier functions for composite energy bands*, Phys. Rev. B **56**, 12847 (1997).
- [129] I. Souza, N. Marzari, and D. Vanderbilt, *Maximally localized Wannier functions for entangled energy bands*, Phys. Rev. B **65**, 035109 (2001).
- [130] G. Pizzi, V. Vitale, R. Arita, S. Blügel, F. Freimuth, G. Géranton, M. Gibertini, D. Gresch, C. Johnson, T. Koretsune, J. Ibañez-Azpiroz, H. Lee, J.-M. Lihm, D. Marchand, A. Marrazzo, Y. Mokrousov, J. I. Mustafa, Y. Nohara, Y. Nomura, L. Paulatto, S. Poncé, T. Ponweiser, J. Qiao, F. Thöle, S. S. Tsirkin, M. Wierzbowska, N. Marzari, D. Vanderbilt, I. Souza, A. A. Mostofi, and J. R. Yates, *Wannier90 as a community code: new features and applications*, J. Phys.: Condens. Matter **32**, 165902 (2020).